General Disclaimer

One or more of the Following Statements may affect this Document

- This document has been reproduced from the best copy furnished by the organizational source. It is being released in the interest of making available as much information as possible.

- This document may contain data, which exceeds the sheet parameters. It was furnished in this condition by the organizational source and is the best copy available.

- This document may contain tone-on-tone or color graphs, charts and/or pictures, which have been reproduced in black and white.

- This document is paginated as submitted by the original source.

- Portions of this document are not fully legible due to the historical nature of some of the material. However, it is the best reproduction available from the original submission.

NSG-7610

Lateral Heterogeneity and Azimuthal Anisotropy of the Upper Mantle: Love and Rayleigh waves 100-250 sec

Toshiro Tanimoto and Don L. Anderson

Seismological Laboratory
California Institute of Technology
Pasadena, California 91125

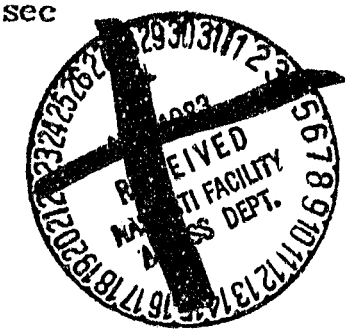

Abstract

The lateral heterogeneity and apparent anisotropy of the upper mantle are studied by measuring Rayleigh and Love wave phase velocities in the period range 100-250 sec. Spherical harmonic descriptions of the lateral heterogeneity are obtained for order and degree up to l=m=10. Slow regions are evident at the East Pacific rise, northeast Africa, Tibet, Tasman sea, southwestern North America and triple junctions in the Northern Atlantic and Indian oceans. Fast regions occur in Australia, western Pacific and the eastern Atlantic. Details which are not evident in previous studies include two fast regions in the central Pacific and the subduction zone in the Scotia Arc region.

Inversion for azimuthal dependence showed (1) little correlation between the fast phase velocity directions and the plate motion vector in plate interiors, but (2) correlation of the fast direction with the perpendicular direction to trenches and ridges. Phase velocity is high when waves propagate perpendicular to these structures. Severe trade-offs exist between heterogeneity and azimuthal dependence because of the yet unsatisfactory path coverage. Confirmation of the azimuthal dependence will require more complete coverage. On the other hand, some details of lateral heterogeneity interpretations may be due to neglected azimuthal variations.

(NASA-CR-174619) LATERAL HETEROGENEITY AND AZIMUTHAL ANISTROPY OF THE UPPER MANTLE: LOVE AND RAYLEIGH WAVES 100-250 SEC Interim Report (California Inst. of Tech.) 35 p HC A03/MF A01 CSCL 08G G3/46

N84-15710

Unclas 15269

1. Introduction

The aims of this paper are to obtain (1) the lateral variation of phase velocity of long period surface waves (100-250 sec) and (2) the azimuthal dependence of phase velocity. We use the spherical harmonic approach. This has the advantage of not requiring an a priori assumption about the nature of the heterogeneity. In practice, we solve for the spherical harmonic coefficients from l=0 to a certain upper limit, lmax. Thus, we can not recover sharp structural discontinuities. Instead, we obtain a long-wavelength averaged structure. This is appropriate, since only long period surface waves are used.

There are two approaches which have been used for the inversion of long period (>100sec) seismograms for lateral heterogeneity of the Earth. One uses waveform inversion and the other uses phase velocity and/or group velocity measurements. The former(Woodhouse, 1983; Woodhouse and Dziewonski, 1983) is probably the most direct approach and fully utilizes the information contained in the seismograms. A disadvantage of this approach is the large storage and computation time required. The velocity method(e.g., Nakanishi and Anderson, 1982, 1983a, 1983b, 1983c) uses only the phase information of the data; the amplitude information is discarded. The measured velocity is the data that the model should satisfy. Measurement of multiplet locations(Silver and Jordan, 1981; Masters *et al.*, 1982) is a varient of this approach, since essentially the same information is obtained and used for inversion. The velocity method requires relatively little storage and computation time.

There are other advantages and disadvantages associated with the two methods. Waveform inversion can treat higher modes easily. It is difficult to isolate modes for phase velocity and group velocity measurements. For the retrieval of azimuthal anisotropy, the velocity measurement approach has the advantage, at least at present, since it is very easy to include in the inversion scheme. Partial derivatives with respect to anisotropy, other than transverse isotropy, have not been derived. These are required in the waveform inversion approach.

In the present study, we attempt to obtain the azimuthal dependence of phase velocity. We also obtain the lateral variation with lmax=10, which is higher than previous studies(e.g., lmax=6 by Nakanishi and Anderson, 1983a,b,c). After presentation of the method, we discuss the problems of least-squares inversion. We examine what the robust features are in the solutions in the singular value decomposition approach and then show the results for various cases.

2. Method

Let t be the travel time of the phase at frequency ω from the source to the receiver and $v(\theta,\varphi,\Psi)$ be the phase velocity as a function of position (θ,φ) and azimuth Ψ. We measure Ψ clockwise from north. We have

$$t = \int_S^R \frac{ds}{v(\theta,\varphi,\Psi)} , \tag{1}$$

where the right hand side is the line integral from the source S to the receiver R. To first order, this is a stationary quantity and the wave path (this line integral) is assumed to be along the great circular path containing S and R.

Phase velocity at (θ,φ), $v(\theta,\varphi,\Psi)$, can be written as

$$v(\theta,\varphi,\Psi) = v_0 + v_h(\theta,\varphi) + v_a(\theta,\varphi,\Psi) , \tag{2}$$

where v_0 is the spherically averaged phase velocity and v_h and v_a are the deviations due to heterogeneity and anisotropy. We assume $|v_h|, |v_a| \ll |v_0|$. Following Backus(1965) and Smith and Dahlen (1973), v_a can be expressed as

$$v_a(\theta,\varphi,\Psi) = a \cos 2\Psi + b \sin 2\Psi + c \cos 4\Psi + d \sin 4\Psi . \tag{3}$$

We substitute (2), (3) in (1), expand the denominator and obtain

$$t = \frac{\Delta_{SR}}{v_0} - \frac{1}{v_0^2}\int_S^R v_h \, ds$$

$$+ \frac{1}{v_0^2}\int_S^R (a \cos 2\Psi + b \sin 2\Psi + c \cos 4\Psi + d \sin 4\Psi) \, ds ,$$

where Δ_{SR} is the distance between S and R. Denoting $\Delta_{SR} - v_0 t = \delta\varphi$ and expanding v_h, a, b, c, and d in terms of spherical harmonics, we get

$$v_0 \, \delta\varphi = \sum_{lm} v_{h\,lm} \int_S^R Y_l^m(\theta,\varphi) \, ds$$

$$+ \sum_{lm} a_{lm} \int_S^R Y_l^m(\theta,\varphi) \cos 2\Psi \, ds + \sum_{lm} b_{lm} \int_S^R Y_l^m(\theta,\varphi) \sin 2\Psi \, ds$$

$$+ \sum_{lm} c_{lm} \int_S^R Y_l^m(\theta,\varphi) \cos 4\Psi \, ds + \sum_{lm} d_{lm} \int_S^R Y_l^m(\theta,\varphi) \sin 4\Psi \, ds , \tag{4}$$

where $v_{h\,lm}$, and a_{lm}, b_{lm}, c_{lm} and d_{lm} are spherical harmonic coefficients of v_h, a, b, c, and d. The left hand side, $v_0 \, \delta\varphi$, is determined from the observation and

we solve systems of equations like (4) for $v_{h\,lm}$, a_{lm}, b_{lm}, c_{lm} and d_{lm}. Note that incorporation of anisotropy 2Ψ and 4Ψ increases the number of unknowns by a factor of five.

For convienience in later sections, we write the system of equations (4) as

$$A\,x = B \tag{5}$$

where

$$x = (v_{h\,00}, v_{h\,10}, \ldots, a_{00}, \ldots, b_{00}, \ldots c_{00}, \ldots, d_{00}, \ldots)^T ,$$

$$B = (v_0\,\delta\varphi\,, \ldots)^T ,$$

and the elements of A are given by line integrals in (4).

3. Data

Phase velocities measured for 15 earthquakes in 1980 (Table 1) from the records of IDA(International Deployment of Accelerometers) and GDSN(Global Digital Seismograph Network) network, are used in this study. The single station method which is used for the measurement is explained in detail in Nakanishi and Anderson (1983c). Source parameters used for the measurement are tabulated in Table 2 (Nakanishi and Kanamori, 1983). The data set is slightly larger than that of Nakanishi and Anderson(1983a,b,c). Only R2 and R3 or G2 and G3 are used for the analysis. Rayleigh and Love waves at periods of 100 sec, 150 sec, 200 sec and 250 sec are analysed and the number of data used in each case is given in Table 3. The number of data for Love waves is less than that of Rayleigh waves since IDA data is restricted to the vertical component.

Path coverage

Figs. 1 and 2 show the path coverage of Rayleigh and Love waves at 200 sec. Overall patterns are very similar at different periods. In both Figs. 1 and 2, the top figure shows the number of surface wave rays that go through each 20°x20° block. The bottom figure shows the azimuthal coverage of rays in each block. The azimuth of a ray can change in a block, thus a mean azimuth is calculated for each ray in a block and shown here.

It is clear from the two figures that coverage of the polar regions is not good, but the area near polar regions is smaller for a given (20°x20°) block size. Path coverage per unit area is better than shown in the figures. Good path

coverages near the Mediterranean, Japan, South Pacific and northern Atlantic ocean correspond to the locations or the antipodes of earthquakes or stations. Spherical harmonic coefficients are mainly controlled by the regions with good coverage. The results in the poorly covered region are essentially extrapolations and should be treated with care.

Overall, path coverage is good, although the azimuthal coverage in some blocks is not. This causes a problem, i.e. trade-off, when azimuthal dependence of phase velocity is incorporated in the inversion. This will be discussed later.

4. Analysis

Solution behavior

First, we solved the system of equations (5) by the conventional least-squares approach, i.e.

$$x = (A^T A)^{-1} A^T R .$$

The solution x becomes very large in some cases. Phase velocity variations exceeded 10 %, which suggests that considerable errors are mapped to a solution due to the near singularity of $(A^T A)$. At this point, we adopted the singular decomposition approach(SVD).

In SVD, A is decomposed as

$$A = U \Lambda V^T ,$$

where U and V are orthogonal matrix and Λ is a diagonal matrix whose elements are eigenvalues of A. Then $(A^T A)^{-1}$ can be written

$$(A^T A)^{-1} = V \Lambda^{-2} V^T .$$

We eliminate some of the smaller eigenvalues in Λ in order to stabilize the solution x. The question then arises; how does the solution change as the number of eigenvalues in Λ kept in the $(A^T A)^{-1}$ (hereafter p) is changed.

Fig.3 shows the solution behaviour of the inversion of Rayleigh waves at 200 sec for heterogeneity with lmax=10. The upper figure shows the solution norm (x) and the residual norm (*). The horizontal axis gives the number of eigenvalues kept (p) and the increment is taken to be 2. The solution norm is defined as the Eulidean norm of the vector x, i.e.

$$|| x || = \sqrt{\sum_i x_i^2},$$

where $x^T = (x_1, x_2, \ldots)$. The residual norm is defined as the Euclidean norm of $Ax - F$.

As p is increased, the residual norm decreases and the resolution becomes better while the solution norm increases. The lower figure shows the behaviour of some of the solutions. Each solution is normalized for plotting purposes. Some of the features shown in this figure are:

(1) There are no drastic changes in the residual and solution norms as p is increased.

(2) Whenever there is a small jump in residual norm and solution norm, the solutions change drastically (for example, see around p=19-23, 63-65, 71-73, and 109-111).

(3) Solution behaviour is especially wild from p=113 to p=121(maximum), which suggests that considerable errors are being mapped into the solution by incorporating these smallest few eigenvalues.

However, even the solution for p=101 showed unrealistically large peaks and troughs, 4-5 %, in the phase velocity variation map. Phase velocity variation of this order, if present, can cause severe multipathing effects(e.g., Sobel and von Seggern, 1978).

Thus we face a problem of the lack of reasonable criterion for the cut-off level, p. This situation does not change for Love waves or for the cases where azimuthal dependence is incorporated. A similar situation for the geomagnetic problem was reported by Whaler and Gubbins(1981). For comparison, the case of Love wave heterogeneity inversion with lmax=10 is shown in Fig. 4.

Effect of the level of eigenvalue cut-off p

With no obvious criterion for selection of p, we can ask the questions 1.) what are the effects of p on the phase velocity variation map and 2.) what are the robust features in the map. Fig. 5 shows the Rayleigh wave heterogeneity inversion at 200 sec with lmax=10. From top to bottom, p is 71, 81, 91 and 101. Contours are drawn at each 0.5 % interval. Striped regions are positive (faster phase velocity) region, while the patterned regions are negative (slower). Zero lines (average velocity) are drawn thicker than other contours.

Three features we can see from this figure are as follows:

(1) The locations of peaks and troughs do not change much as p is changed. Note, for example, the troughs (slower regions) in northeastern Africa, Tibet, near Fiji and New Zealand and the East Pacific rise to California and the peaks (faster regions) in the western Pacific, Australia, northeastern Pacific and western Africa to northwestern part of Asia. These features seem to be quite robust.

(2) Although the locations are robust, the total variation increases as p is increased.

(3) The shape of the zero contour changes, as p is changed.

The same conclusions can be reached from Fig.6, which shows the results of Love wave heterogeneity inversions at 200 sec with lmax=10. In this figure, p is 47, 53, 59 and 71 from top to bottom.

Effect of windowing

Once the spherical harmonic coefficients are obtained, some kind of window should be applied to these coefficients in order to avoid the ringing phenomena associated with truncation at lmax. Effects of windowing are shown in Fig. 7. The case of Love waves at 200 sec with lmax=10 and p=53 is used in this figure.

The top figure corresponds to the Hamming window, i.e.

$$w(l) = 0.54 + 0.46 \cos\left(\frac{\pi}{\text{lmax}} l\right) . \qquad (6)$$

The same w(l) is applied to all coefficients within the same angular order l.

The other three figures correspond to the windowing by the function

$$w(l) = \cos\left(\frac{\pi}{2} \frac{l}{\text{lmax} + n}\right) . \qquad (7)$$

The parameter n is 1, 2 and 4 for the second, third and fourth figure from top. The effect of changing n is similar to the effect of changing the level of cut-off p, i.e. the locations of peaks and troughs do not change much but the zero contour changes as different windows are applied. As higher l coefficients become less suppressed, more details emerge. For example, a positive peak in the central Pacific in the top three figures is broken up into two peaks in the bottom figure. This is done, of course, at the risk of introducing spurious ringing in the map.

We use the window of the bottom figure for all other figures in this paper unless otherwise noted.

5. Results and discussion

In this section, we show the results of inversions with and without the azimuthally dependent terms. In all cases, we set the eigenvalue cut-off level p, such that the solution norm does not exceed 0.008. This has the effect of setting the maximum value of the phase velocity variations at about 2-2.5 %. As discussed in the last section, maximum values are not robust features of a solution but locations of peaks and troughs are.

Results for heterogeneity inversion

We present the results for lmax=10 in this paper. Azimuthal dependence is not yet taken into account. The total number of parameters is $(lmax+1)^2 = 121$ in this case. The numbers of eigenvalues kept in the solution are given in the first row of Table 4. Larger p means better resolution. Rayleigh waves have better resolution than Love waves and in both cases the best resolution is achieved at 200 sec.

Fig. 8 shows the results for Love waves. The results for 100 sec, 150 sec, 200 sec and 250 sec are given from top to bottom. There are excellent correlations with surface tectonics. Generally, old oceans and shields have fast phase velocities, while ridge regions and marginal seas have slow velocities. Subduction zones are generally characterized by slow velocity, which is presumably the effect of slow velocity in the back-arc regions.

There are gradual changes from 100 sec to 200 sec, but the map for 250 sec is quite different. There is, for example, a slow peak south of Africa, which does not exist clearly in the top three figures. Also, a fast peak occurs in the western Pacific and the fast peak in the northeastern Pacific disappeared. Moreover, the locations of the peaks have shifted.

There is a possibility that this is due to the relatively poor fit of the model to the data. As shown in the first row of Table 5a, the total variance reduction (TVR) at 250 sec is not as good as TVR at other periods. TVR is calculated by $TVR = (\sigma_0^2 - \sigma^2)/\sigma_0^2$, where σ_0^2 is the variance for the spherically symmetric Earth and σ^2 is the variance for the aspherical model obtained by inversion. But we do not think this is likely to be the cause for this case, since comparable difference of TVR exists between 150 sec and 200 sec without much difference in

locations of peaks. It is more likely to be caused by heterogeneity in deeper regions of the upper mantle, which is not correlated with shallower features.

The results for Rayleigh waves are given in Fig. 9. There are quite a few similarities with the Love wave results. For example, slow velocities in the Red Sea-Gulf of Aden region to the triple junction in the south Indian ocean, Tibet, East Pacific rise to California and Tasman Sea to New Zealand. Australia and the eastern Atlantic are fast in both sets of maps.

At the same time, there exist some differences. The fast regions in the western Pacific are shifted somewhat. The Canadian shield is fast for Love waves and slow for long-period Rayleigh waves. Ridges are generally slow for Love waves but they are not so evident on Rayleigh wave maps. Some ridge segments are, in fact, fast for Rayleigh waves. Subduction zones are characterized by slow velocity for Love waves but some are fast for Rayleigh waves at long periods.

In terms of path coverage, Rayleigh waves have much better coverage than Love waves (Figs. 1 and 2). Nakanishi and Anderson(1983c) discussed the problem of source depth errors on Rayleigh wave initial phase. However, TVR of Rayleigh waves is larger than that of Love waves(Tables 5a and 5b). Thus it is more likely that the data should be explained by differences in penetration depth or transverse isotropy. Differences in subduction zones, slow for Love waves and fast for Rayleigh waves, are probably due to the difference in penetration depth, since fast velocity at depth is consistent with the subduction of cold, fast lithosphere. Love wave-Rayleigh wave differences at trenches and ridges can also be caused by transverse isotropy. This is because SH may be less than SV due, presumably, to ascending and descending flow in the mantle (Anderson and Regan, 1983), although in general SH > SV in the shallow mantle (Anderson and Dziewonski, 1982).

Compared with previous studies by Nakanishi and Anderson(1983a, b, c; lmax=6), the overall patterns are very similar: slow regions at the East Pacific Rise, northeast Africa, Tibet, Tasman Sea, southwestern North America and triple junctions in the north Atlantic and south Indian Ocean and fast regions at Australia, western Pacific and the Eastern Atlantic. But a few detailed features have emerged. Most notable is the break-up of the fast regions in the Pacific. This appears clearly for Love waves at 100 sec, 150 sec and 200 sec and Rayleigh waves at 150 sec and 200 sec. In terms of the numbers of data and the variance reductions (TVR), the results at 150 sec and 200 sec are most reliable (Tablas 5a and 5b). Thus we believe that this apparent increase in resolution is real.

Another feature is the slow region in the southeast Pacific, which extends into the Scotia Sea for short period Love waves.

Results for azimuthal dependence

When azimuthal dependence is included, the number of parameters increases considerably. For heterogeneity plus 2Ψ azimuthal inversion, there are three times as many parameters and for heterogeneity plus 2Ψ and 4Ψ terms, there are five times as many parameters. Thus lmax has to be decreased from 10 and we mainly discuss the results for lmax=6 with 2Ψ dependence in this paper. Even for this case, we have 145 parameters. Maximum l, lmax, is taken to be the same for both heterogeneity and azimuthally dependent terms in (4). However, l=0 is excluded from the azimuthally dependent terms.

Figs. 10 and 11 show the results for Love and Rayleigh waves respectively for lmax=6 with 2Ψ dependence. The lines on the maps give the direction of fastest phase velocity at each point. The length of each line gives the difference of velocity between the fastest and the slowest velocity at a point.

For both Love and Rayleigh waves, the fastest directions do not correlate well with plate motion vectors. The map for Rayleigh wave at 100 sec seems to have the best correlation, particularly for the Pacific and Australian plates. Since Love waves at 100 sec period sample the shallowest parts of the Earth among the cases in Figs. 10 and 11, this case should have the best correlation, if the fast direction is the spreading direction. However, there is little correlation.

On the other hand, the fast direction is generally nearly perpendicular to plate boundaries. This can be seen along the mid-Atlantic ridge, western America, subduction zones in the western Pacific and the ridges in the Indian Ocean. This may indicate that the azimuthally dependent phase velocity is caused by lateral heterogeneity rather than azimuthal anisotropy. It is natural to expect that velocities are different depending upon whether waves propagate along or perpendicular to ridges and slabs.

It is also possible that anisotropic crystals, such as olivine, are oriented or recrystallized by the high stresses and high temperatures at plate boundaries and that the fast directions correlate with the stress field. Dziewonski and Anderson (1983) suggest a correlation of anisotropy with stress. In any event, our results indicate that anisotropy is not uniform under a given plate. Uniform flow is not expected when both plate drag and counterflow are taken into account (Hager and O'Connell, 1978; Chase, 1979).

We need much more data before we can be fully confident of our azimuthal results and the above discussion should be viewed in this light. There is a trade-off between heterogeneity and anisotropy. Figs. 12a and 12b show results for Love waves obtained by inversion with and without the 2Ψ azimuthally dependent terms respectively. Periods are 100 sec, 150 sec, 200 sec and 250 sec from top to bottom. In both cases, lmax is taken to be 6. The cut-off level of eigenvalues are listed in Table 4 with other cases of inversion, lmax=4.

Comparisons of Figs. 12a and 12b reveal that the locations of peaks and troughs are not so different, but definitely there exists trade-off, since the maximum values in Fig. 12a are much smaller. TVR calculated for Fig. 12a are 40.0, 38.0, 45.9 and 36.3 % from top to bottom and those for Fig. 12b are 36.3, 36.8, 41.6 and 33.5 %. In Table 5a and 5b, we list the variance reductions due to heterogeneity (HVR) for inversions with azimuthally dependent terms. HVR for Fig. 12a are 30.7, 29.1, 33.5 and 25.1 %. Thus at 100 sec , for example, out of the total variance reduction of 40.0 %, 30.7 % is explained by heterogeneity and the rest by azimuthal dependence. Care should be taken with these numbers, since they are not quite additive. But it is clear that there exist severe trade-offs between heterogeneity and azimuthal dependence.

In Table 5a and 5b, we show the results of the inversions for lmax=4 with 2Ψ dependence and with 2Ψ and 4Ψ dependence. For Love waves at 100 sec, for example, TVR increases from 32.1 % to 35.2% by including 4Ψ terms but HVR decreases from 23.4% to 17.8%. This feature can be seen for all cases, i.e. TVR increase slightly by incorporating 4Ψ terms in the inversion but HVR decrease quite dramatically. In general, in order to retrieve high azimuthal dependence, good azimuthal path coverage is required. The above results suggest that the azimuthal coverage of our data set is not yet complete enough to recover both the 2Ψ and 4Ψ terms of the azimuthal anisotropy.

6. Conclusions

Using phase velocities measured for 15 earthquakes in 1980, lateral variation of phase velocity and its azimuthal dependence were obtained. Because the matrix in the normal equation is nearly singular, singular value decomposition is used instead of the least-squares approach. After examining the truncation level of eigenvalues and the effect of windowing, the locations of peaks and troughs were shown to be robust but the maximum values are not.

Inversion for heterogeneity showed two new features. The fast regions in the central Pacific are resolved into several smaller anomalies. A Scotia arc anomaly has been identified. The overall patterns, however, are similar to previous studies with lower lmax.

Inversion for azimuthal dependence shows little correlation between the fastest velocity directions and the plate motion vectors. The fastest directions are generally perpendicular to ridges and trenches. The phase velocity is slower when waves propagate along ridges and trenches. At the same time, however, severe trade-off between azimuthal dependence and heterogeneity was shown to exist due to the yet unsatisfatory path coverage. Thus, confirmation of the results for azimuthal dependence should be awaited until more data are incorporated into the inversion. The relation of azimuthal anisotropy to return flow in the upper mantle will be discussed in a separate paper.

Acknowledgement

We wish to thank Ichiro Nakanishi for listening to our ideas and kindly supplying his data. The IDA data used were made available to us by courtesy of the IDA project team at the Institute of Geophysics and Planetary Physics, University of California. This research was supported by NSF grant No. EAR811-5236 and NASA grant No. NSG-7610. Contribution number 3993, Division of Geological and Planetary Sciences, California Institute of Technology, Pasadena, California 91125.

REFERENCES

Anderson, D. L. and Regan, J., Uppermantle anisotropy and the oceanic lithosphere, *Geophys. Res. Lett.*, *10*, 841-844, 1983.

Anderson, D. L. and Dziewonski, A. M., Upper mantle anisotropy:evidence from free oscillations, *Geophys. J. R. Astr. Soc.*, *69*, 383 404, 1982.

Backus, G. E., Possible forms of seismic anisotropy of the upper mantle under oceans, *J. Geophys. Res.*, 70, 3429-3429, 1965.

Chase, C. G., Asthenospheric counterflow: a kinematic model, *Geophys. J. R. Astr. Soc.*, *66*, 1-18, 1979.

Dziewonski, A. M. and Anderson, D. L., Travel times and station corrections for P waves at teleseismic distances, *J. Geophys. Res.*, *88*, 3295-3314, 1983.

Hager, B. H. and O'Connell, Kinematic models of large-scale flow in the Earth's mantle, *J. Geophys. Res.*, *84*, 1031-1048, 1979.

Masters, G., Jordan, T. H., Silver, P. G., and Gilbert, F., Aspherical earth structure from fundamental spheroidal-mode data, *Nature*, *298*, 609-613, 1982.

Nakanishi, I. and Anderson, D. L., World-wide distribution of group velocity of mantle Rayleigh waves as determined by spherical harmonic inversion, *Bull. Seism. Soc. Am.*, *72*, 1185-1194, 1982.

Nakanishi, I. and Anderson D. L., Aspherical heterogeneity of the mantle from phase velocities of mantle waves, *Nature*, in press, 1983a.

Nakanishi, I., and Anderson, D. L., Measurements of mantle wave velocities and inversion for lateral heterogeneity and anisotropy, Part I: Analysis of Great Circle Phase Velocities, submitted to *J. Geophys. Res.*, 1983b.

Nakanishi, I., and Anderson, D.L., Measurements of mantle wave velocities and inversion for lateral heterogeneity and anisotropy, Part II: Analysis by the single-station method, submitted to *Geophys. J. R. astr. Soc.*, 1983c.

Nakanishi, I., and Kanamori, H., Source mechanisms of twenty-six large shallow earthquakes (M_s> 6.5) during 1980 from P-wave first motion and long-period Rayleigh wave data, submitted to *Bull. Seism. Soc. Am.*, 1983.

Silver, P. G., and Jordan, T. H., Fundamental spheroidal mode observations of aspherical heterogeneity, *Geophys J. R. astr. Soc.*, *64*, 605-634, 1981.

Sobel, P. A. and von Seggern, D. H., Applications of surface-wave ray tracing, *Bull. Seism. Soc. Am.*, *68*, 1359-1380, 1978.

Smith, M. L. and Dahlen, F. A., The azimuthal dependence of Love and Rayleigh wave propagation in a slightly anisotropic medium, *J. Geophys. Res.*, *78*, 3321-3333, 1973.

Whaler, K. A. and Gubbins, Spherical harmonic analysis of the geomagnetic field: an example of a linear inverse problem, *Geophys. J. R. astr. Soc*, *65*, 645-693, 1981.

Woodhouse, J. H., The joint inversion of seismic waveforms for lateral variations in Earth structure and earthquake source parameters, in+ Proceedings of the Enrico Fermi International School of Physics, LXXXV (H. Kanamori and E. Boschi, eds.), North Holland, in press, 1983.

Woodhouse, J. H., and Dziewonski, A. M., Mapping the upper mantle: Three dimensional modelling of Earth structure by inversion of seismic waveforms, submitted to *J. Geophys. Res.*, 1983.

FIGURE CAPTIONS

Fig. 1: The upper figure shows the number of surface wave rays in each 20°x20° block. The lower figure shows the azimuthal coverage of rays in each block. This is for Rayleigh wave at 200 sec. Path coverages are similar for 100 sec, 150 sec and 250 sec.

Fig. 2: same as Fig. 1 except that this is for Love wave at 200 sec.

Fig. 3: Solution behaviour of heterogeneity inversion with lmax=10. This is for Rayleigh waves at 200 sec. The upper figure shows the residual norm(*) and the solution norm(x) as a function of the number of eigenvalues kept (p) in the solution. they are plotted from 11 to 121 at an interval of 2. The lower figure shows the behaviour of the solutions. Their behaviour is wild for $p>90$ and especially so for $113 \leq p \leq 121$.

Fig. 4: Same as Fig. 3 except for Love wave at 200 sec.

Fig. 5: Effect of the level of eigenvalue cut-off, p. This is for Rayleigh wave heterogeneity inversion with lmax=10 at 200 sec. From top to bottom, p is 71, 81, 91 and 101. Locations of peaks and troughs of phase velocities do not change much, while the maximum values increase as p is increased. Contour interval for this and all other maps is 0.5%.

Fig. 6: Same as Fig. 5 except for Love waves. From top to bottom, p is 47, 53, 59 and 71.

Fig. 7: Effect of windowing. The top figure is the result of Hamming window (equation 6) and the rest are the results of windowing by the function in (7). The parameter n is 1, 2 and 4 for the second, third and fourth figure. The window with n=4 is used for all other figures in this paper.

Fig. 8: Results of Love wave heterogeneity inversion with lmax=10. The results at 100 sec, 150 sec, 200 sec and 250 sec are shown from top to bottom.

Fig. 9: Same as Fig. 8 except for Rayleigh waves.

Fig. 10: Results of inversion with azimuthally dependent terms for Love waves. The 2Ψ terms as well as heterogeneity terms with lmax=6 are inverted. Plotted in this figure are the fastest direction of phase velocity at each point. Length of lines specify velocity difference between the fastest direction and the slowest (perpendicular) direction. From top to bottom, periods are 100 sec, 150 sec, 200 sec and 250 sec.

Fig. 11: Same as Fig. 10 except for Rayleigh waves.

Fig. 12a: Phase velocity variation obtained by Love wave inversion with 2Ψ azimuthally dependent terms. Azimuthal dependence obtained simultaneously

is shown in Fig. 10. Ir this and the next figures (Fig. 12b), no window is applied.

Fig. 12b: Results of Love wave heterogeneity inversion with lmax=6. Locations of peaks and troughs are similar with Fig. 12a, but their maximum values are much higher. This shows the existence of trade-off in the inversion between heterogeneity and azimuthal depedence.

Table 1
List of Earthquakes (in 1980) Used

No.	m	d	h	m	s	Lat.	Lon.	Ms	Region
1	1	1	16	42	40.0	38.815N	27.780W	6.7	Azores
3	2	7	10	49	16.0	54.158S	158.890E	6.5	Macquarie Islands
4	2	23	5	51	3.2	43.530N	146.753E	7.0	Kurile Islands
7	3	24	3	59	51.3	52.969N	167.670W	6.9	Fox Islands
8	6	9	3	28	18.9	32.220N	114.985W	6.4	Cal-Mex Border
12	7	8	23	19	19.8	12.410S	166.381E	7.5	Santa Cruz Island
14	7	14	16	15	1.7	20.273S	177.154W	6.6	Kermadec
16	7	29	3	11	56.3	13.101S	166.338E	6.7	Vanuatu Islands
19	10	10	12	25	23.5	36.195N	1.354E	7.3	Algeria
21	10	25	7	0	7.9	21.982S	170.025E	6.7	Loyalty Island
22	10	25	11	0	5.1	21.890S	169.853E	7.2	Loyalty Island
24	11	8	10	27	34.0	41.117N	124.253W	7.2	N. California
26	11	23	18	34	53.6	40.914N	15.366E	6.9	Italy
27	12	17	16	21	58.8	49.479N	129.496W	6.8	Vancouver Island
28	12	31	10	32	11.0	46.060N	151.453E	6.5	Kurile Islands

Table 2

Source parameters of the earthquakes used

No.	depth(km)	τ	$M_o(x10^{20})$	δ	λ	φ
1	9.75	17.2	2.38	86.2	3.0	-31.0
3	9.75	29.7	1.9	84.0	0.0	-70.0
4	43.0	19.3	6.31	70.0	89.2	27.0
7	33.0	30.1	2.95	60.0	88.1	53.3
8	9.75	15.4	0.465	90.0	180.0	140.1
12	33.0	51.4	21.5	59.0	93.1	170.0
14	43.0	18.0	1.38	70.0	82.9	10.0
16	43.0	19.1	1.57	54.0	93.5	160.0
19	9.75	30.2	4.89	54.0	81.8	225.0
21	33.0	38.7	9.30	74.0	93.2	143.0
22	33.0	46.8	29.2	73.0	88.2	142.0
24	16.0	31.7	10.3	90.0	0.0	49.8
26	9.75	44.7	2.94	63.0	275.8	-43.0
27	9.75	26.2	1.54	90.0	180.0	-37.1
28	33.0	27.8	2.90	68.0	89.6	28.3

KEY:

τ - rise time (sec)

M_o - seismic moment (dyne cm)

δ - dip angle (deg)

λ - slip angle (deg)

φ - strike, measured clockwise from north (deg)

Table 3

Number of data used for analysis

Period (sec)	Rayleigh	Love
100	497	369
150	562	385
200	577	380
250	557	356

Table 4

The level of eigenvalue cut-off(p) for each case of inversion

		Love				Rayleigh			
lmax	Anisotropy	100	150	200	250	100	150	200	250
10		43	53	54	53	49	65	82	74
4	2Ψ	29	30	28	36	35	42	52	49
4	$2\Psi + 4\Psi$	34	37	37	43	47	56	63	62
6	2Ψ	40	40	43	46	52	55	63	63

Table 5a

Love waves: total variance reduction(TVR) and variance reduction by heterogeneity (HVR)

		100		150		200		250	
lmax	Anisotropy	TVR	HVR	TVR	HVR	TVR	HVR	TVR	HVR
		(%)		(%)		(%)		(%)	
10		40.5		39.3		44.1		36.7	
4	2Ψ	32.1	23.4	34.5	22.4	41.6	31.5	33.3	21.4
4	$2\Psi + 4\Psi$	35.2	17.8	37.6	16.1	43.7	22.9	36.0	13.2
6	2Ψ	40.0	30.7	38.0	29.1	45.9	33.5	36.3	25.1

Table 5b

Rayleigh waves: total variance reduction(TVR) and variance reduction by heterogeneity (HVR)

		100		150		200		250	
lmax	Anisotropy	TVR	HVR	TVR	HVR	TVR	HVR	TVR	HVR
		(%)		(%)		(%)		(%)	
10		45.8		64.9		66.6		54.5	
4	2Ψ	40.3	36.3	56.9	38.6	57.1	37.8	45.9	18.6
4	$2\Psi + 4\Psi$	41.3	32.3	60.1	34.2	60.1	35.9	47.9	23.9
6	2Ψ	42.7	37.7	64.4	52.3	64.0	48.4	50.4	35.8

15	19	22	22	26	27	20	14	13	13	15	16	20	19	16	14	11	8
42	41	32	38	33	32	41	41	38	66	69	44	38	38	38	38	46	47
129	128	72	110	69	71	87	170	72	57	86	132	139	63	100	71	92	94
107	56	44	49	67	117	98	93	41	42	61	58	92	65	45	67	103	156
61	58	46	37	52	86	77	93	85	64	55	43	37	59	94	73	94	99
51	67	60	76	63	57	66	139	246	102	66	47	48	58	142	108	77	49
43	73	96	101	78	74	71	98	127	145	95	73	72	73	83	79	93	56
56	68	63	36	42	39	39	51	69	55	47	46	44	36	36	40	55	50
17	20	24	25	24	23	22	15	14	19	20	25	27	30	30	27	20	14

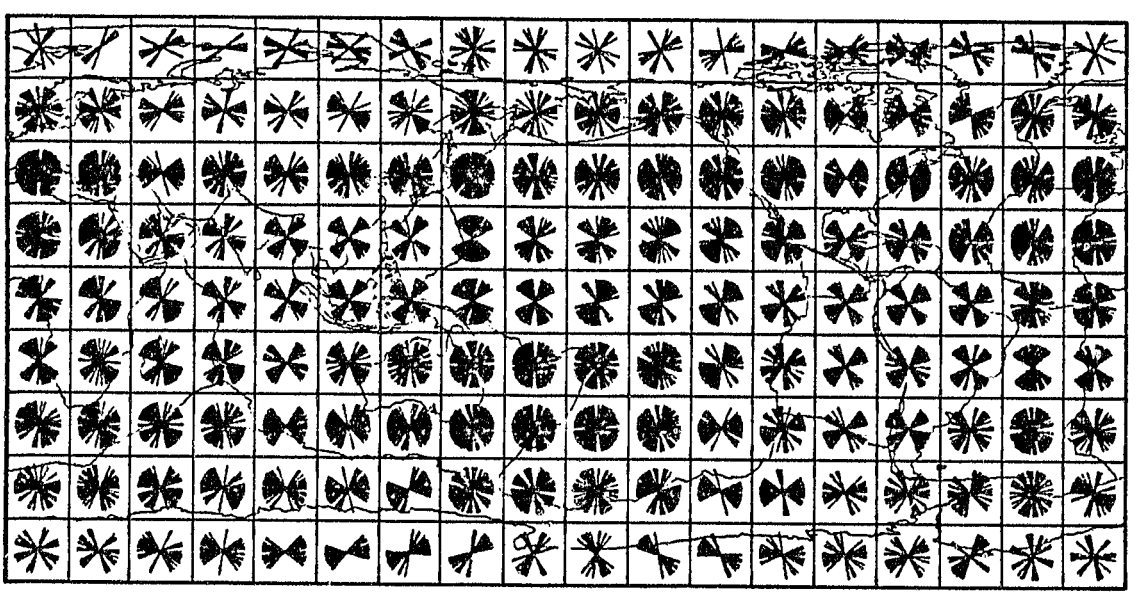

Fig. 1

9	15	18	18	20	21	12	7	8	7	8	6	7	8	9	8	6	7
40	40	28	29	24	27	33	24	20	35	24	20	18	18	18	19	30	28
126	98	52	69	40	46	58	114	45	27	37	76	77	32	46	34	50	57
64	32	28	34	44	76	64	85	26	13	27	35	51	40	32	49	63	93
34	39	23	19	36	59	48	62	48	33	37	24	19	43	68	47	62	57
20	39	34	40	40	41	49	91	142	82	31	28	32	40	87	60	54	27
18	29	56	54	40	47	41	47	81	100	65	53	51	44	31	51	66	32
31	31	33	23	22	21	17	33	49	43	40	36	32	26	26	34	36	27
9	9	8	9	8	9	11	10	11	13	16	20	20	22	22	19	10	7

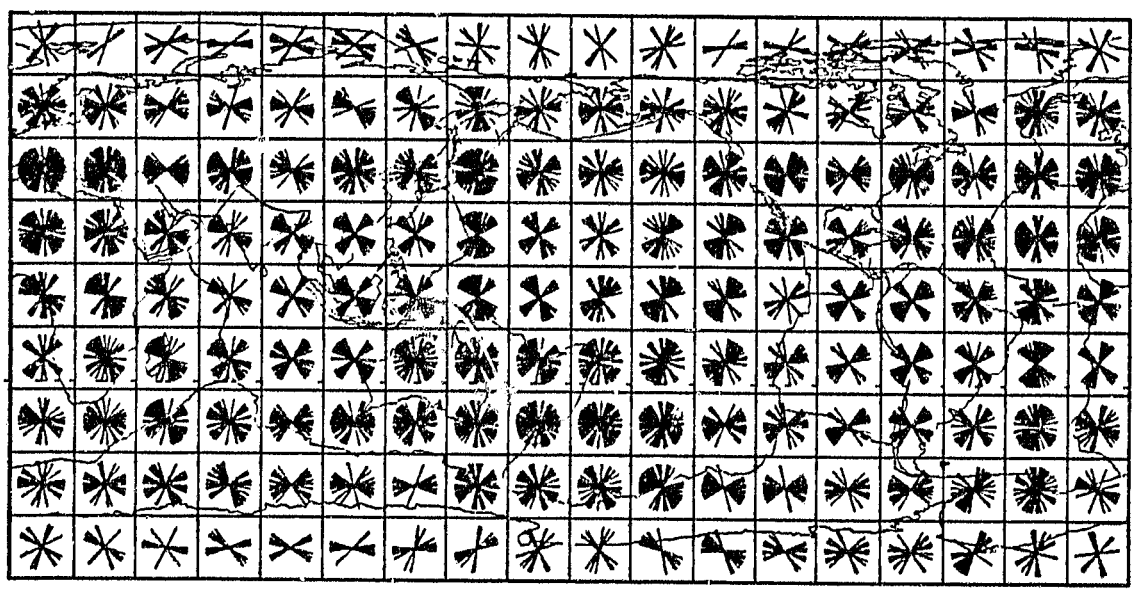

Fig. 2

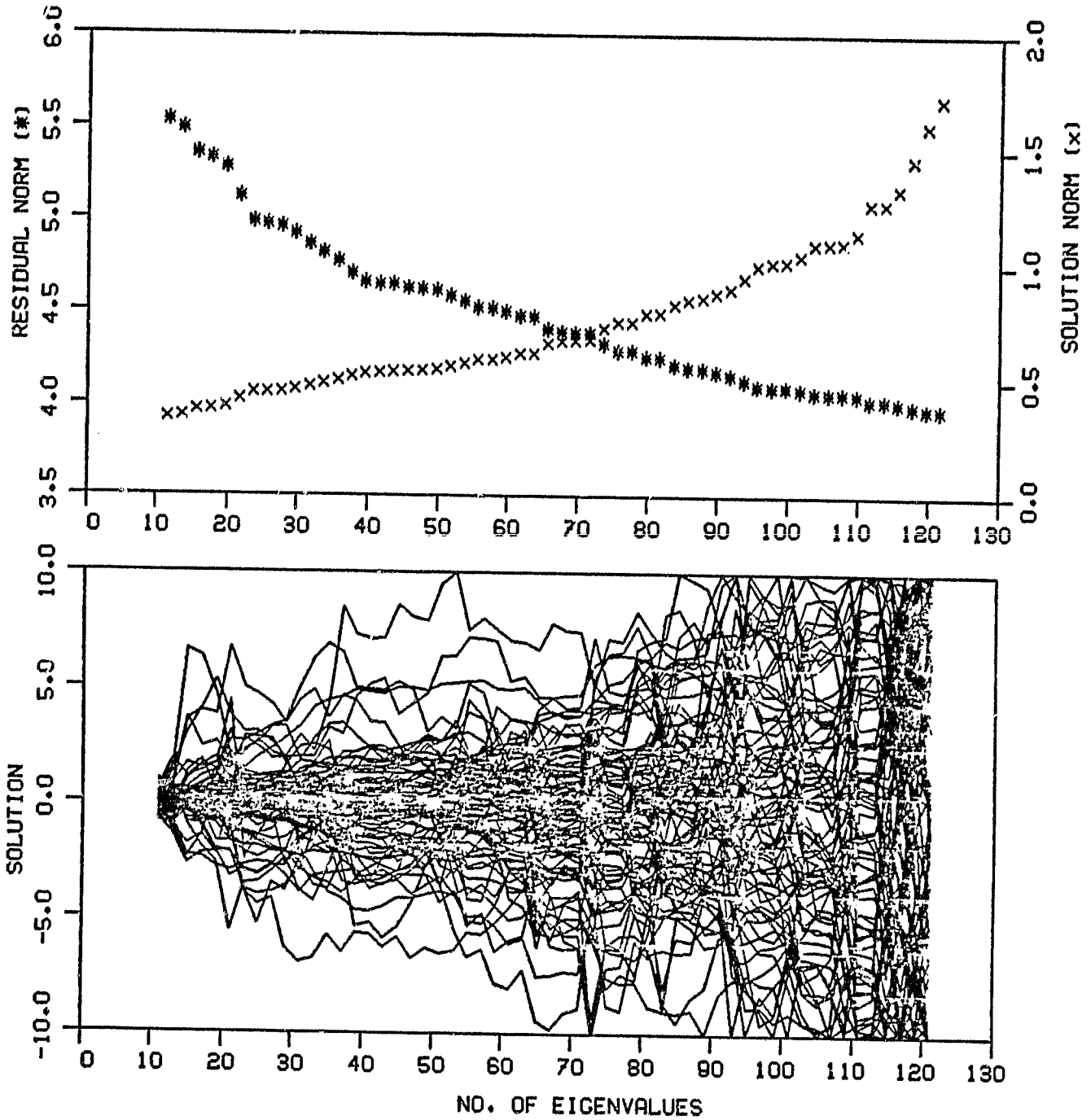

Fig. 3

ORIGINAL PAGE IS
OF POOR QUALITY

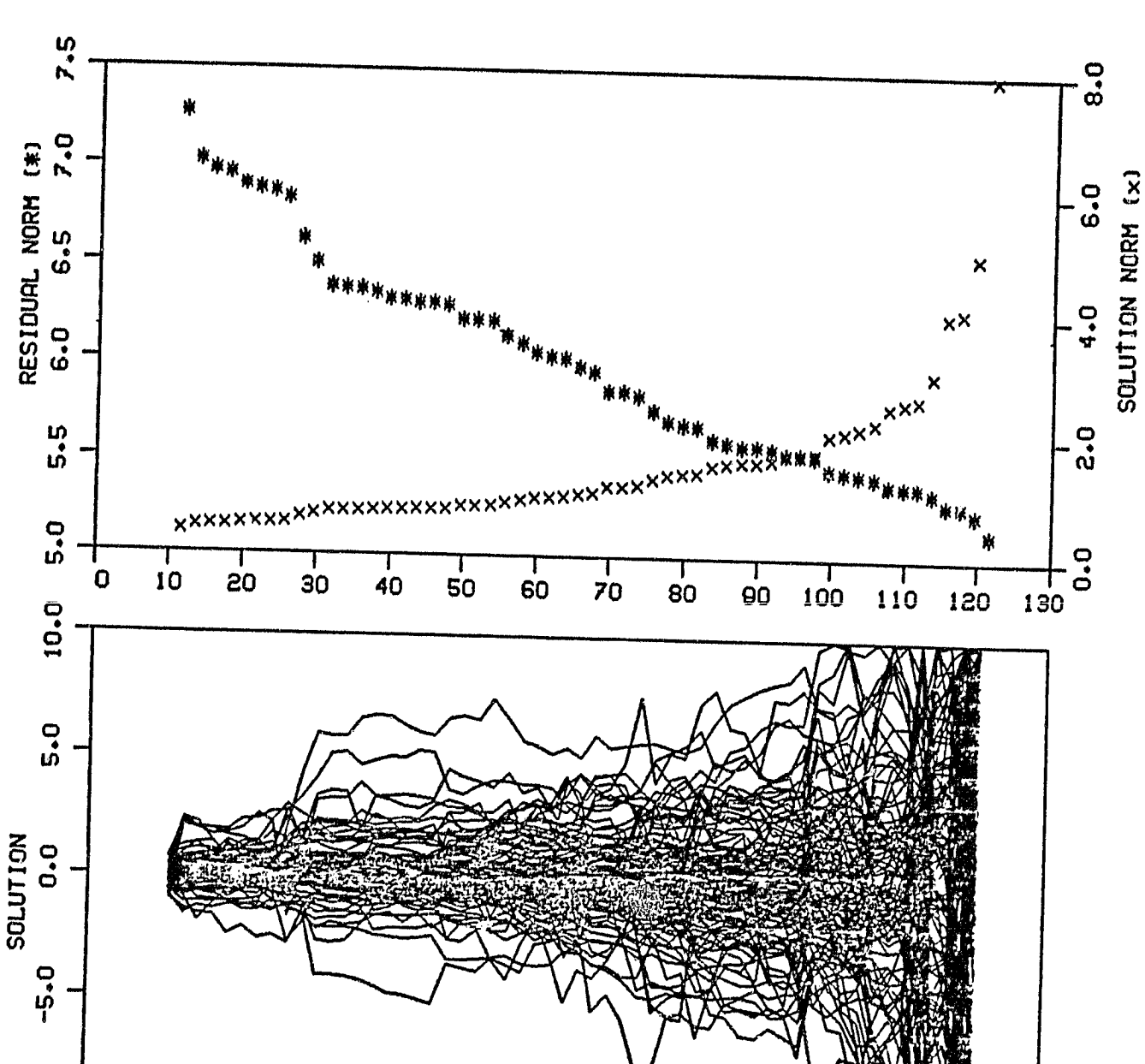

Fig. 4

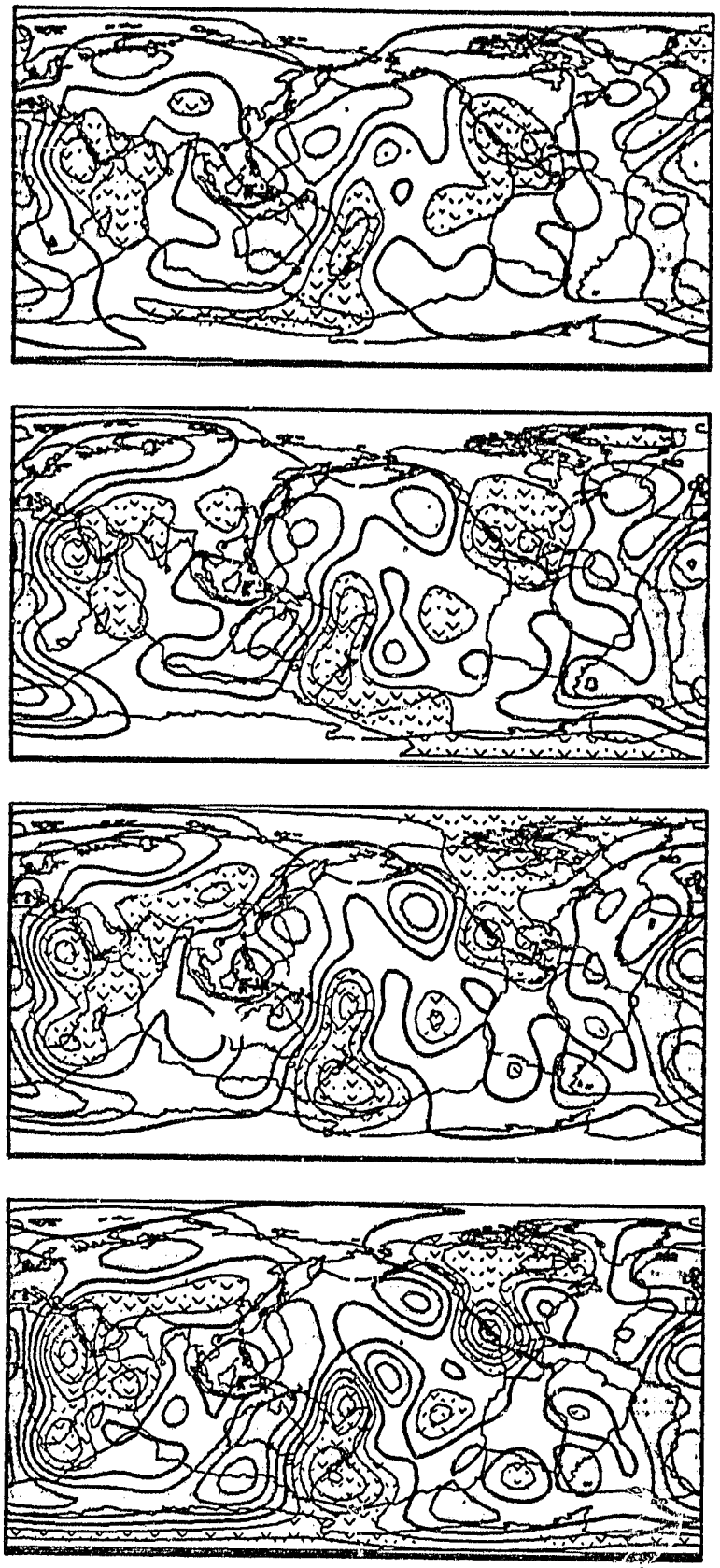

Fig. 5

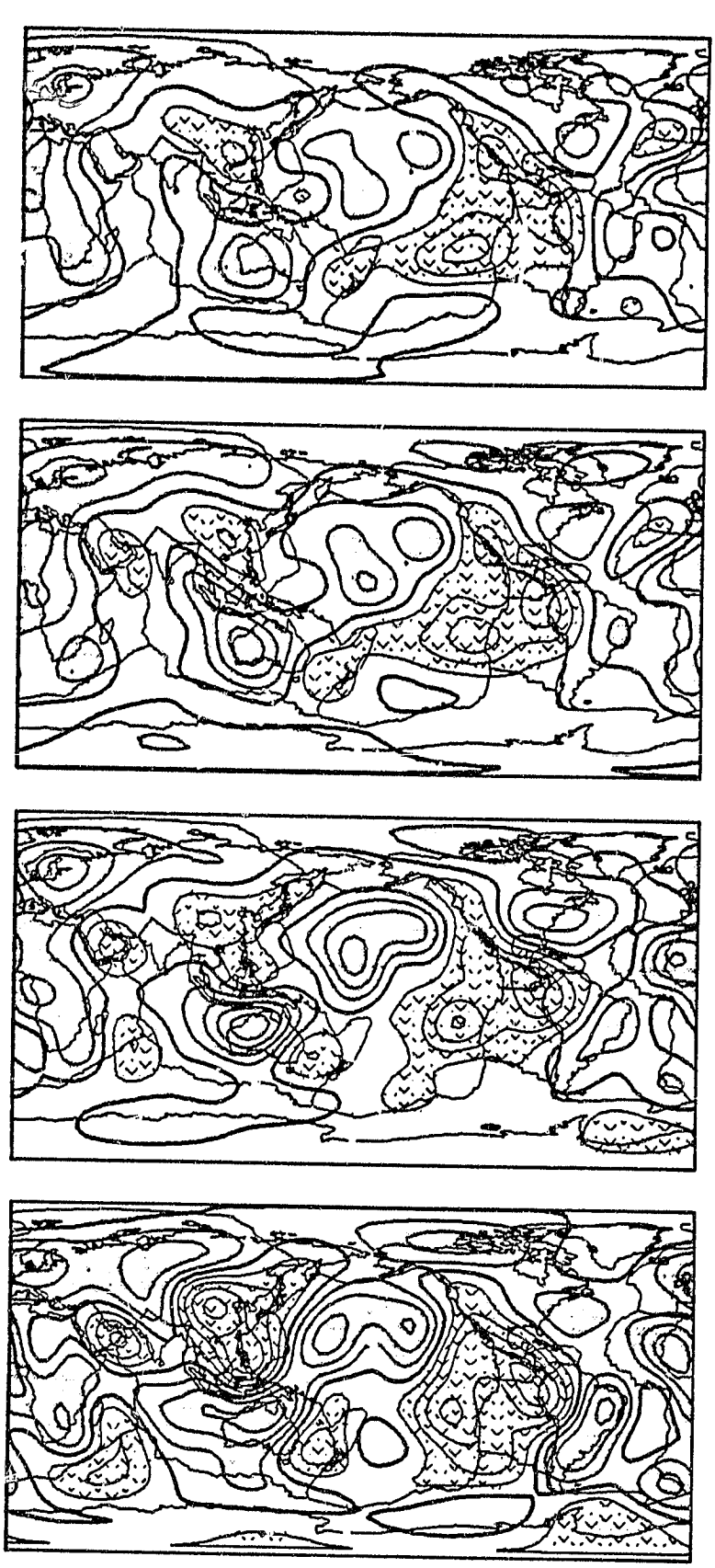

Fig. 6

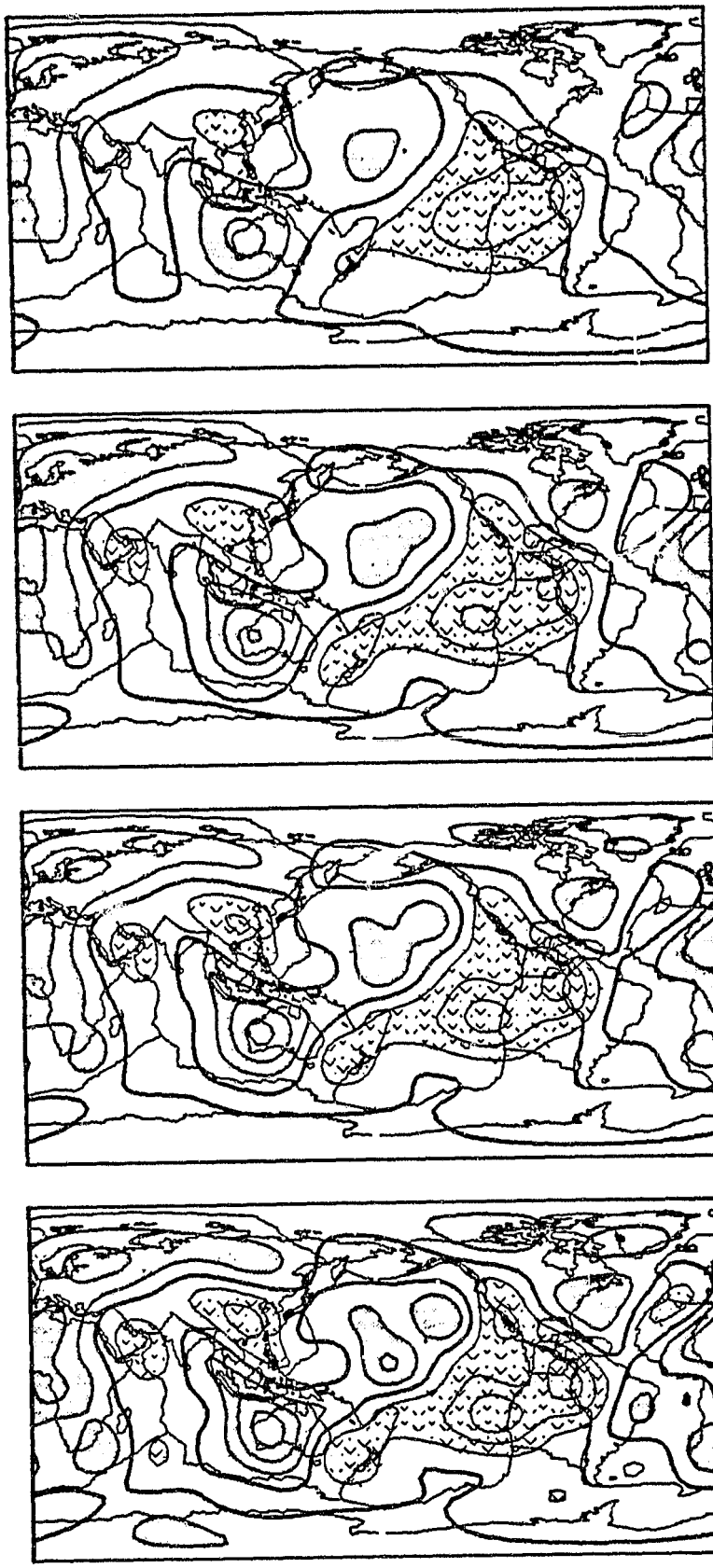

Fig. 7

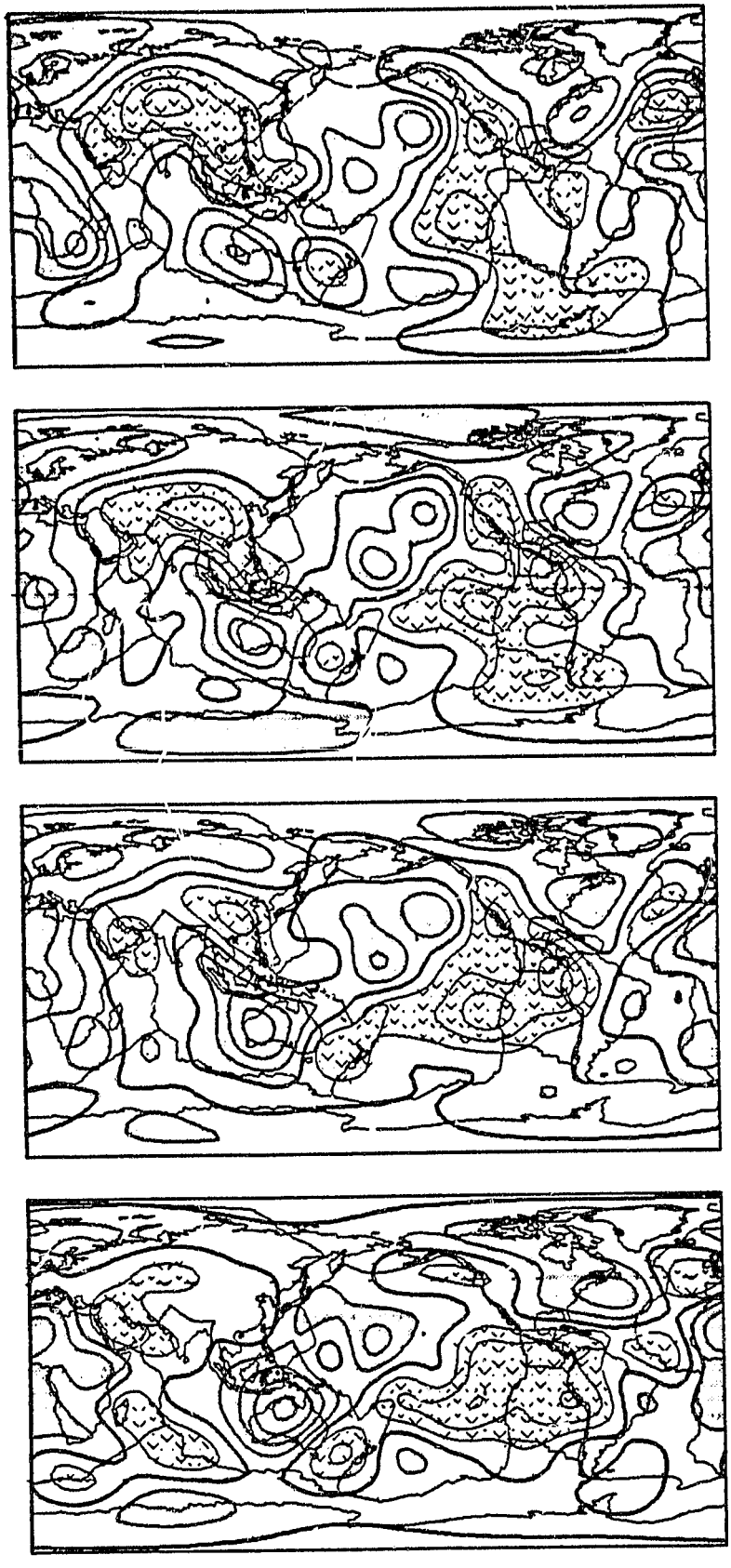

Fig. 8

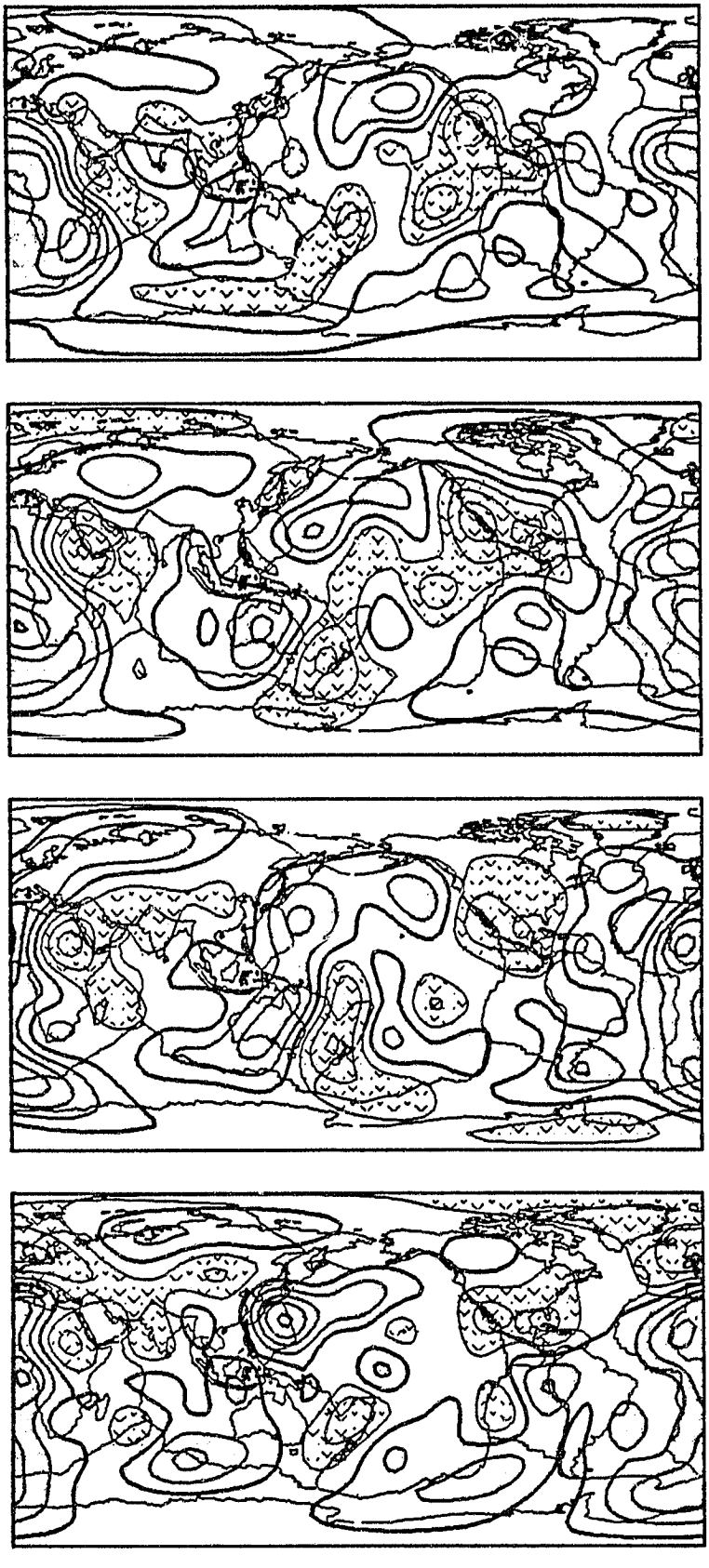

Fig. 9

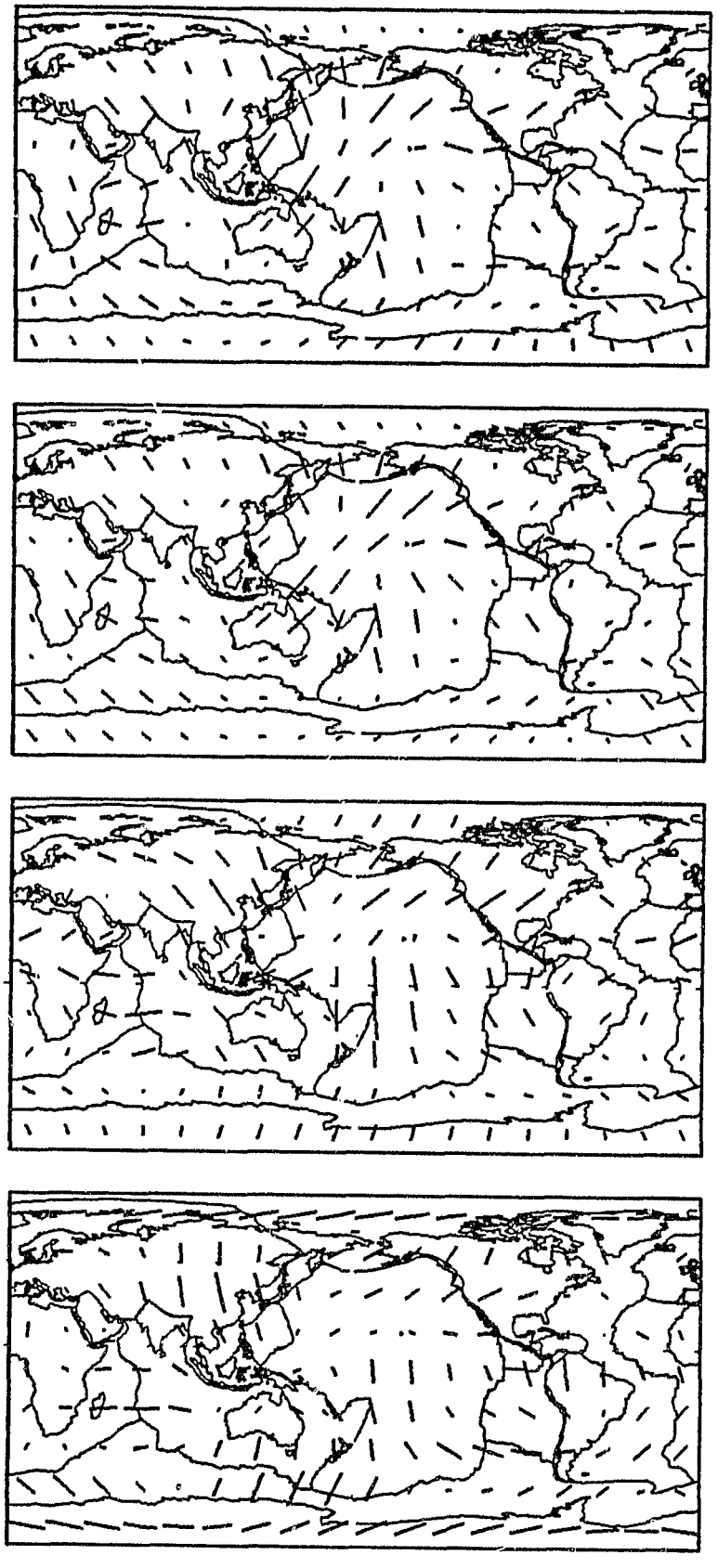

— 1 per cent

Fig. 10

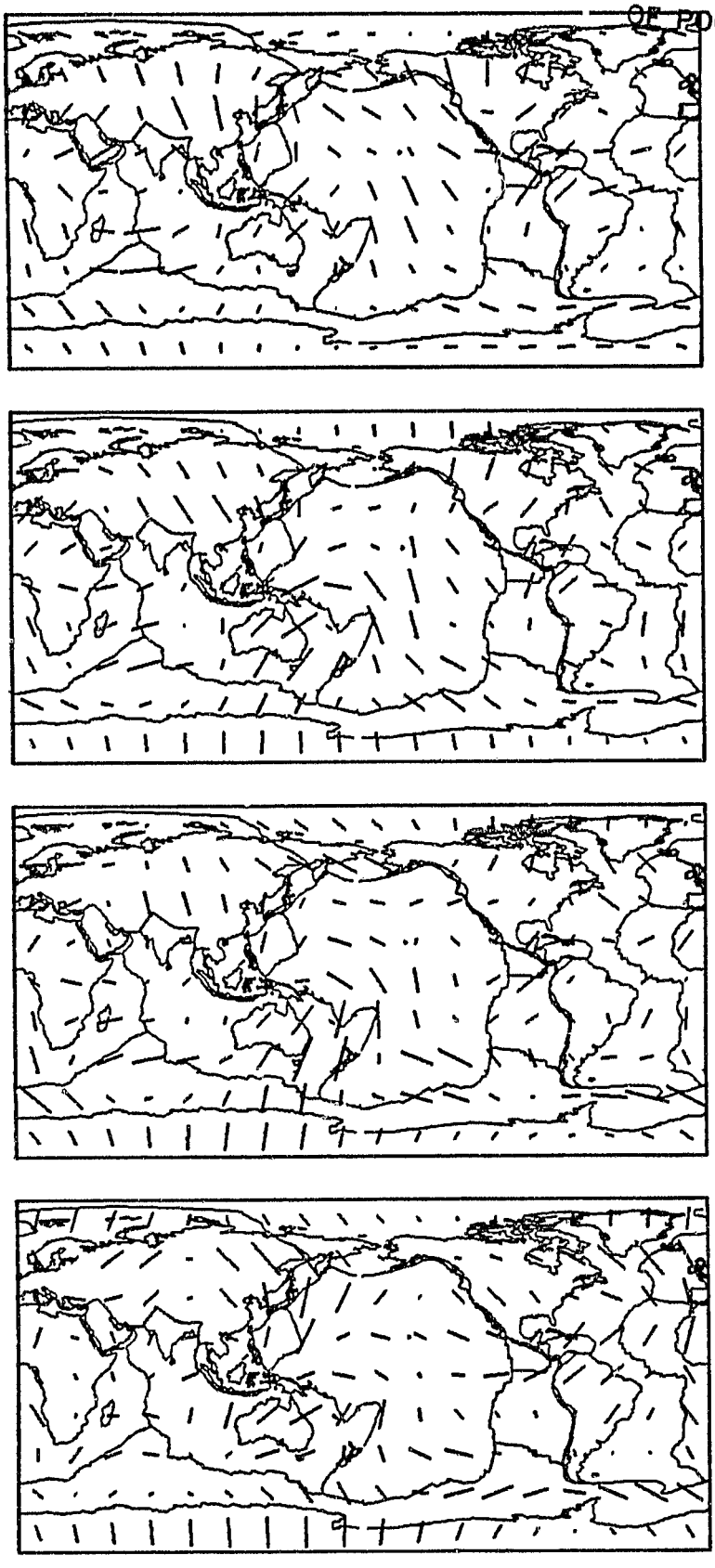

— 1 per cent

Fig. 11

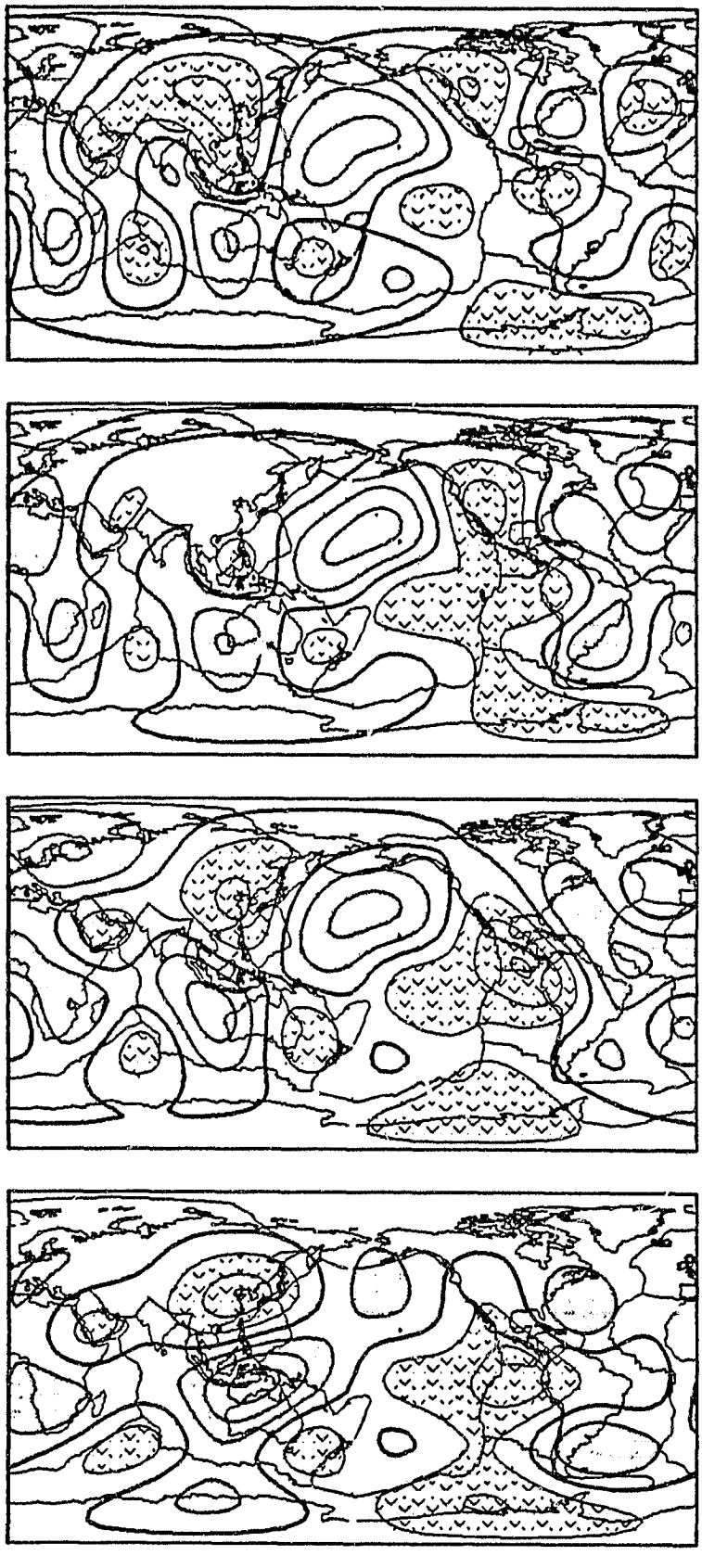

Fig. 12a

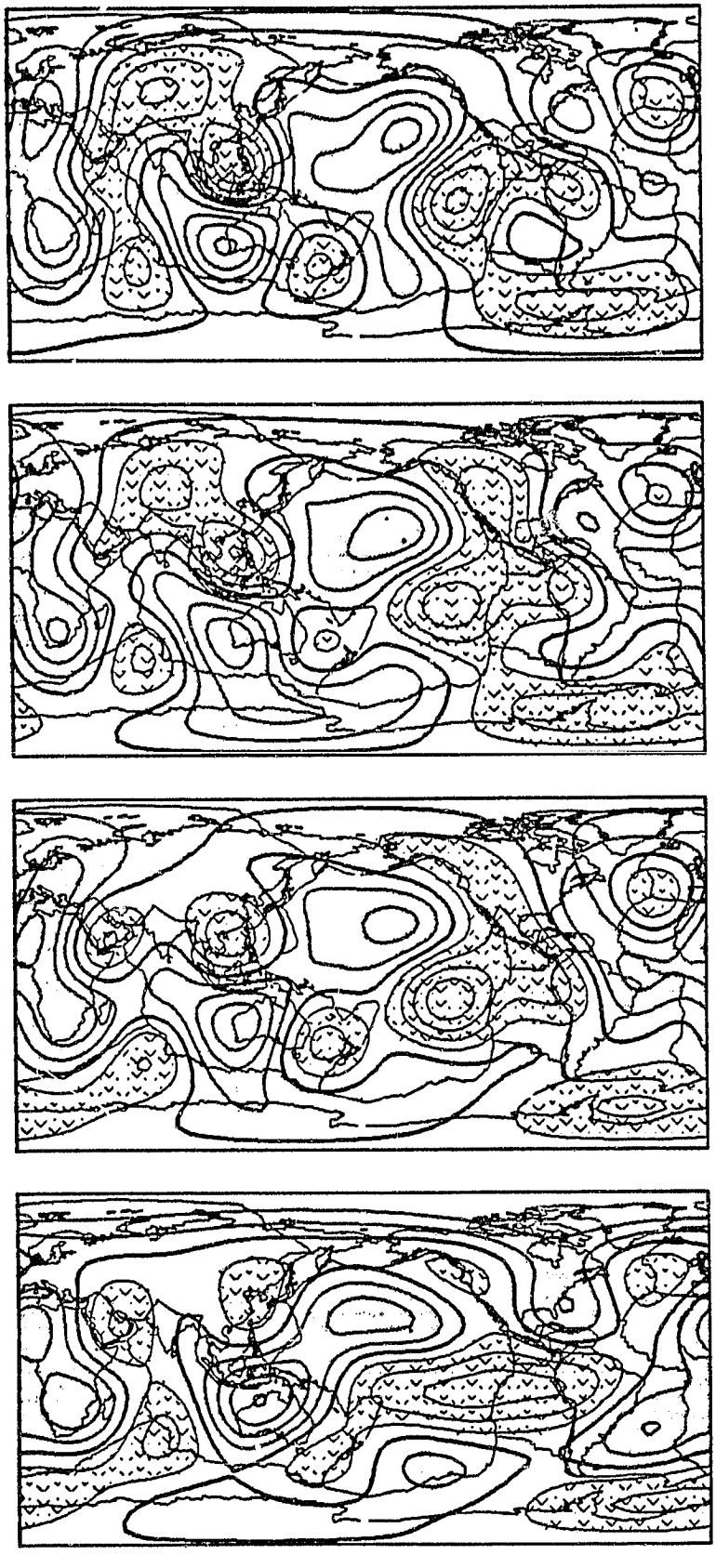

Fig. 12b